Physico-Chemical and Electrochemical Properties of Platinum–Tin Nanoparticles Synthesized by Pulsed Laser Ablation for Ethanol Oxidation

ARTICLE *in* THE JOURNAL OF PHYSICAL CHEMISTRY C · AUGUST 2008

Impact Factor: 4.77 · DOI: 10.1021/jp801143a

4 AUTHORS, INCLUDING:

Mohamed Mohamedi
Institut national de la recherche scientifique
105 PUBLICATIONS **1,971** CITATIONS
SEE PROFILE

Daniel Guay
Institut national de la recherche scientifique
245 PUBLICATIONS **4,764** CITATIONS
SEE PROFILE

Physico-Chemical and Electrochemical Properties of Platinum−Tin Nanoparticles Synthesized by Pulsed Laser Ablation for Ethanol Oxidation

Pascale Bommersbach, Mohamed Chaker, Mohamed Mohamedi, and Daniel Guay*

Institut National de la Recherche Scientifique (INRS), Énergie, Matériaux et Télécommunications, 1650 Boulevard Lionel Boulet, Varennes, Quebec, Canada J3X 1S2

Received: February 7, 2008; Revised Manuscript Received: June 27, 2008

Mixed Pt−Sn catalysts were prepared by crossed beam pulsed laser deposition. Five catalyst compositions were investigated, namely, $Pt_{100}Sn_0$, $Pt_{90}Sn_{10}$, $Pt_{75}Sn_{25}$, $Pt_{50}Sn_{50}$, and $Pt_{30}Sn_{70}$. The depositions were performed either under vacuum or in the presence of 2 Torr He. The pressure in the deposition chamber has a strong influence on the surface structure and morphology of the catalytic particles, as determined from scanning electron micrographs (SEM) and atomic force microscopy (AFM). For catalysts prepared under He, X-ray diffraction (XRD) patterns show an expansion of the fcc lattice, indicating that Sn atoms are dissolved in it. Up to 13 atom % Sn can be dissolved in the Pt fcc structure. In contrast, less than 3 atom % of Sn can be dissolved in Pt when the catalysts are prepared under vacuum. X-ray photoelectron spectroscopy has revealed that the surface composition of Pt_xSn_{100-x} catalysts prepared under 2 Torr He closely follows the bulk concentration. Catalysts with the same composition prepared under vacuum exhibit a surface enrichment with Pt atoms. In these catalysts, tin is highly oxidized and the mean [O]/[Sn] surface ratio is 2.35. In contrast, tin in catalysts prepared under 2 Torr He is less oxidized and the mean [O]/[Sn] surface ratio is 1.37. Cyclic voltammogram curves reveal that mixing Sn with Pt lowers the onset oxidation potential of ethanol. This effect is more pronounced for catalysts prepared under 2 Torr He, and $E_{onset} = 0.31$ V vs RHE is reached for $[Pt]_{bulk} = 75$ atom %. Similarly, chronoamperometric measurements conducted at +0.5 V vs RHE also demonstrated that $Pt_{75}Sn_{25}$ catalyst prepared under 2 Torr He is the most active after 1 h of electrolysis. The reasons underlying these differences are discussed.

1. Introduction

Direct alcohol fuel cells (DAFCs) use methanol or ethanol as fuel directly without external reformer, which makes them simple and compact.[1,2] Unlike methanol, which is known to be toxic for human and animal life, ethanol is a particularly promising and interesting alternative as a renewable fuel which can be produced in large quantities from biomass. The complete electro-oxidation of ethanol to CO_2 is difficult to achieve, and pure platinum is not the most efficient anodic catalyst for direct ethanol fuel cells (DEFCs). During the oxidation of ethanol, platinum is poisoned by reaction intermediates and its activity deteriorates with time. To counter this problem, platinum is often mixed with a second metal (like Ru, Pb, Sb, Rh, Sn, etc.) to enhance its electrocatalytic activity and tolerance to poisoning by reaction intermediates.

Several authors have investigated mixed Pt−Sn catalysts for the (partial) electro-oxidation of ethanol, and superior performances were obtained compared to pure Pt.[3−23] The procedure followed to prepare Pt−Sn catalysts has a marked influence on the composition and structure of the resulting material and, consequently on its electrocatalytic activity toward ethanol oxidation. One of the most popular synthesis procedures is the reduction of Pt and Sn by appropriate reducing agents.[4−13] Other methods have also been used; for example, Lamy et al. relied on the Bönneman method[14−16] to prepare mixed Pt−Sn catalysts, while Gonzalez et al. preferred to use a suspension technique.[17,18]

Physical deposition methods have also been investigated for Pt−Sn catalyst preparation.[19,22,24] For example, we showed recently that sputter deposition is a very effective way of adding Sn to Pt to improve the electrocatalytic activity of the resulting material toward ethanol oxidation.[19] Other physical deposition methods like pulsed laser deposition can also be used to prepare mixed Pt−Sn catalysts, and it is worthwhile to investigate them in the search for better ways to prepare more efficient electrocatalysts for ethanol oxidation.

In this study, a series of Pt_xSn_{100-x} catalysts was prepared by pulsed laser deposition (PLD). PLD is a deposition technique well adapted for the synthesis of complex nanomaterials.[25] Several deposition parameters can influence the structure and properties of the deposited materials.[26,27] Thus, it is of utmost importance to understand how the deposition conditions impact on the electrocatalytic response of the resulting materials. In this work, our attention was focused on the influence of the background pressure in the deposition chamber. For this, catalysts with different compositions (Pt_xSn_{100-x}) were synthesized under vacuum or in a He atmosphere. Scanning electron microscopy (SEM), energy-dispersive X-ray (EDX), atomic force microscopy (AFM), X-ray diffraction (XRD), and X-ray photoelectron spectroscopy (XPS) techniques were used to characterize the catalysts. Their electrocatalytic activities for ethanol oxidation were also evaluated by performing cyclic voltammetry and chronoamperometric measurements.

2. Experimental Methods

2.1. Catalyst Preparation. The Pt−Sn catalysts were deposited by crossed beam pulsed laser ablation by means of a pulsed KrF excimer laser ($\lambda = 248$ nm, pulse width = 17 ns, and repetition rate = 50 Hz). Pure platinum (99.99%, Kurt J.

* To whom correspondence should be addressed.

10.1021/jp801143a CCC: $40.75
Published on Web 08/22/2008

Lesker Co.) and tin (99.998−99.999%) (Kurt J. Lesker Co.) targets were used. The targets were moved continuously across the laser beam (via a dual rotation and translation motion) to obtain a uniform ablation over the entire target surfaces. A schematic description of the experimental setup has been given elsewhere.[28]

Prior to deposition, the chamber was evacuated by means of a turbo pump (4×10^{-5} Torr). Helium was then introduced in the deposited chamber. In this study, samples were prepared either under vacuum or in the presence of He at a fixed background pressure (2 Torr). In all cases, the substrate-to-target distance was fixed at 5 cm. The choice of performing the deposition under a fixed He background pressure is based on a previous study that showed that $Pt_{75}Sn_{25}$ catalysts prepared in these conditions displayed the best electrocatalytic activity for ethanol oxidation.[27] The [Pt]/[Pt] + [Sn] concentration ratio of the catalyst was adjusted by independently varying the laser fluence on the two targets.

The substrates consist of disks made of graphite (99.997%, Ø = 5 mm, Goodfellow Corp.) that were previously polished and cleaned with a solution of hexane and ethylacetate. Then, they were heated at 100 °C in air for 1 h.

2.2. Scanning Electron Microscopy and Energy-Dispersive X-ray Analysis. Scanning electron microscopy (SEM) micrographs were obtained using a JSM-6300F microscope at an accelerating voltage of 20 kV. The Pt and Sn bulk chemical compositions were determined by energy-dispersive X-ray (EDX) analysis. Throughout this paper, the notation Pt_xSn_{100-x} was used to indicate the bulk atomic composition of the catalyst.

2.3. Atomic Force Microscopy. The surface morphology and roughness of the samples were investigated by atomic force microscopy (AFM) using a Nanoscope III microscope from Digital Instrument. The mean roughness (R_q) was calculated according to the following equation

$$R_q = \sqrt{\frac{\sum (Z_i - Z_{ave})^2}{N}}$$

where Z_i is the height at (x_i, y_i) and Z_{ave} is the average height.

2.4. X-ray Diffraction. The crystalline structure of all samples was determined by X-ray diffraction (XRD) using Bruker D8 Advance diffractometer equipped with a Cu Kα source. The diffractometer was operated at 40 kV and 40 mA. All diffractograms were acquired in the $\theta-2\theta$ scan mode with an angular step size of $2\theta = 0.04°$ and an acquisition time of 20 s by step.

2.5. X-ray Photoelectron Spectroscopy. X-ray photoelectron spectroscopy measurements were performed using a VG Escalab 220i-XL equipped with an Mg Kα source (1253.6 eV). The anode was operated at 10 kV and 20 mA. The pass energy of the analyzer was fixed at 20 eV. All samples were analyzed with a spot size of 250 × 1000 μm located approximately in the center of the sample. A survey spectra ranging from 0 to 1000 eV was first acquired, and then higher resolution multiplex scan spectra (Pt 4f, O 1s, C 1s, and Sn 3d core levels) were obtained. Quantification of the elements was performed with CasaXPS software (Casa Software Ltd.) by fitting the core level spectra after a Shirley background removal.[29] The metallic components of the Pt 4f region were fitted using a Gaussian/Lorentzian asymmetrically modified line shape, while a Gaussian/Lorentzian line shape was used to fit the other components. The C 1s core level peak at 284.6 eV, resulting from hydrocarbon contaminants at the surface, was used as an internal reference. All spectra have been recalibrated with respect to the C 1s core level peak of adventitious carbon contamination.

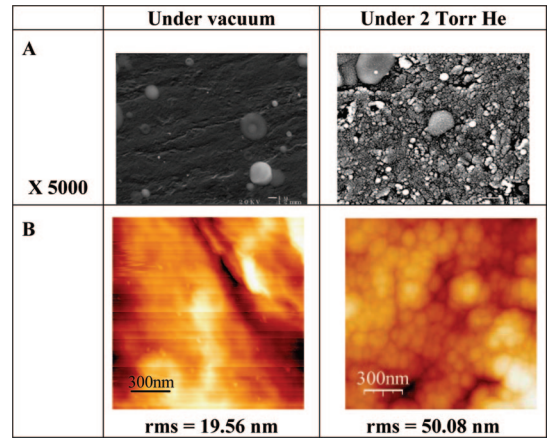

Figure 1. Scanning electron microscopy (SEM) micrographs (A) and atomic force microscopy (AFM) images (B) of $Pt_{75}Sn_{25}$ electrodes elaborated under vacuum and 2 Torr He.

2.6. Electrochemical Study. Electrochemical studies were carried out in a deaerated solution of H_2SO_4, 0.5 M + C_2H_5OH, 1 M. A reference hydrogen electrode (RHE) was used, and the counter electrode was a platinized Pt plate. Current−potential ($I-E$) and chronoamperometric ($I-t$) curves were measured with a potentiostat EG&G model 273A. Prior to the electrochemical measurements in ethanol, the surface of the working electrode was cleaned electrochemically by potential cycling in H_2SO_4, 0.5 M. Before each test, dissolved oxygen was removed from the solution by bubbling argon for 15 min. All electrochemical measurements were carried out at room temperature. The current densities are referred to the geometric surface area of the electrodes (i.e., 0.2 cm^2). In some instances, the current densities were also normalized with respect to the electrochemically accessible surface area (EASA). This was done by recording the CVs of the catalysts (in H_2SO_4) at several scan rates between 0.45 and 0.65 V vs RHE and computing the capacitance of the electrode from the variation of the current with respect to the sweep rate. A value of 20 $\mu F\ cm^{-2}$ metal atoms was then used to calculate the EASA.

3. Results

3.1. SEM-EDX Analysis. SEM micrographs of all samples were recorded to investigate the electrode morphology, and only the most representative examples are presented. Figure 1A and 1B shows the SEM images of $Pt_{75}Sn_{25}$ catalysts prepared under vacuum and 2 Torr He, respectively. Samples prepared under vacuum display a smooth surface with a few scattered particles dispersed on the sample surface. The largest ones have a diameter of ∼2 μm, and the smallest ones have a diameter of a few hundred nanometers. It was determined by EDX analysis that most of these particles are made of tin. Care was taken to avoid including these particles for determination of the Pt bulk composition of the catalyst. Samples prepared under 2 Torr He have a different morphology. In that case, the surface is made of an ensemble of small particles, all having a similar diameter.

3.2. AFM Analysis. Figure 1C and 1D shows the AFM images of $Pt_{75}Sn_{25}$ catalysts prepared under vacuum and 2 Torr He, respectively. The AFM image of Figure 1C is structureless. The mean roughness, R_q, is close to 20 nm. In the case of Figure 1D, distinctive particles are observed on the surface. The mean diameter of these particles is 20 nm, and the mean roughness is larger than 50 nm, an increase of 250% compared to samples prepared in vacuum. As we shall see later, the mean crystallite

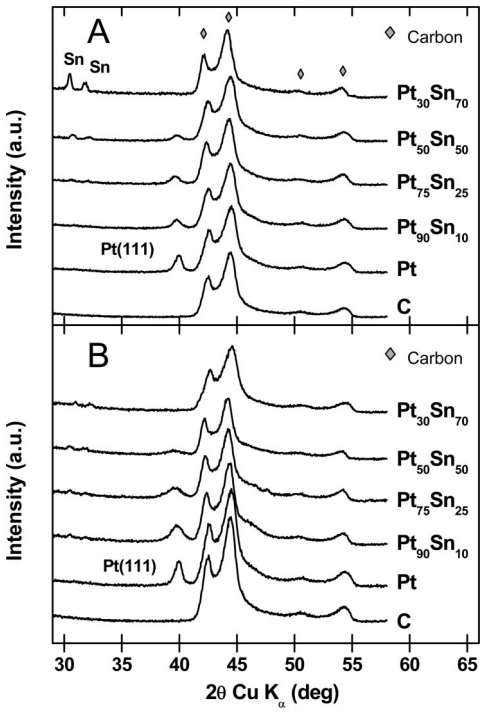

Figure 2. X-ray diffraction patterns of Pt_xSn_{100-x} catalysts deposited under vacuum (A) and 2 Torr He (B). The bulk catalyst compositions are indicated on the right-hand side of the curves.

size determined by X-ray diffraction is close to 10 nm, indicating that the particles seen by AFM are indeed aggregates of smaller crystallites.

3.3. XRD Analysis. The XRD patterns of Pt_xSn_{100-x} catalysts deposited in vacuum and under 2 Torr He are shown in Figure 2A and 2B, respectively. Five different catalyst compositions were investigated, namely, $Pt_{100}Sn_0$, $Pt_{90}Sn_{10}$, $Pt_{75}Sn_{25}$, $Pt_{50}Sn_{50}$, and $Pt_{30}Sn_{70}$. For the sake of comparison, the XRD pattern of the graphitic carbon substrate is also shown.

The most important diffraction peaks of the substrate occur at $2\theta = 42.2°$, 44.3°, 50.4°, and 53.9°, while those of tin are at $2\theta = 30.6°$, 32.0°, 43.9°, 44.9°, and 55.3° (Sn(200), Sn(101), Sn(220), Sn(211), and Sn(301), respectively). As seen in Figure 2A and 2B, metallic tin is present in the catalyst with low Pt content. The intensity of these peaks is more important in the case of catalyst prepared in vacuum, indicating that the phase proportion of tin is higher in these films. As far as we can tell, there are no diffraction peaks in the vicinity of $2\theta = 34°$ and 52° that could be indexed to SnO_2 (101) and (211) peaks, respectively, indicating that bulk crystalline SnO_2 is not formed during the deposition process. However, the presence of a small amount of crystalline or amorphous form of tin oxides cannot be totally excluded.

In the case of Pt, the most intense diffraction peaks are the (111) and (200) peaks that occur at $2\theta = 39.8°$ and 46.4°, respectively. The first one is well separated from those of the graphitic support, while the second one is weak and cannot be easily differentiated from them. Also, it is important to note that the Sn diffraction peaks do not interfere with the Pt(111) peak. Thus, the Pt(111) diffraction peak was chosen to evaluate the lattice parameter of the fcc phase. The position of the Pt(111) diffraction peak extracted from the XRD patterns of the various catalysts is given in Table 1.

The variation of the Pt fcc lattice parameter, a, with the bulk composition of the Pt_xSn_{100-x} catalysts is shown in Figure 3A. As depicted in that figure, the lattice parameter varies with the

TABLE 1: Peak Position and Average Crystallite Size of Pt_xSn_{100-x} Catalysts

	under vacuum		under 2 Torr He	
catalyst	2θ (deg)	crystallite size (nm)	2θ (deg)	crystallite size (nm)
Pt	39.90	14.8	39.88	
$Pt_{90}Sn_{10}$	39.80	13.5	39.79	9.3
$Pt_{75}Sn_{25}$	39.75	12.3	39.66	8.5
$Pt_{50}Sn_{50}$	39.78	13.4	39.40	7.9

bulk composition and the background pressure in the deposition chamber. For Pt_xSn_{100-x} prepared in vacuum, a increases from 3.91 to ~3.92 Å as the Pt bulk content is reduced from 100 to 90 and then stays constant at ~3.92 Å for lower Pt content. In contrast, for Pt_xSn_{100-x}, a increases linearly from 3.91 to ~3.96 Å as the bulk Pt content decreases from 100 to 50. The increase of the lattice parameter a as the Pt bulk content is decreased indicates that Sn is dissolved in the fcc phase of Pt and that a true solid solution is formed.[5,7,9,11,12,17,18,20]

In the literature, conflicting conclusions have been reached on the composition and microstructure of bimetallic Pt−Sn catalyst. Kuznetsov et al.[30] reported that platinum forms practically all possible alloys with tin. However, in some cases, PtSn (1:1) was the only alloy phase formed,[31] even when the Pt/Sn mole ratio was varied from 1:1 to 1:10.[32] A minor contribution from a $PtSn_2$ phase was sometimes observed by electron microdiffraction, but the other Sn-containing phases could not be identified.[33,34] High-resolution transmission electron microscopy allowed Davis and co-workers to conclude that the dominant alloy formed on an alumina support was PtSn and that a significant fraction of other alloys like Pt and Pt_3Sn were present only at low Sn/Pt ratios.[35] More recently, Radmilovic et al.[36] conducted a high-resolution transmission electron microscopy study on bimetallic Pt−Sn catalysts deposited on a carbon support. They showed that catalysts with a 1:1 Pt/Sn

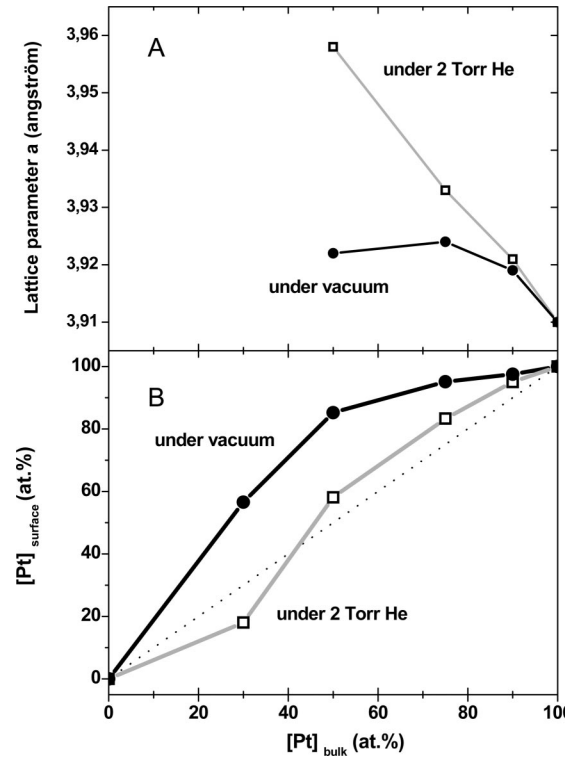

Figure 3. Variation of the lattice parameter (A) and Pt surface composition (B) of Pt_xSn_{100-x} catalysts as a function of the Pt bulk concentration.

atomic ratio heat treated at 500 °C contained a Pt-rich fcc alloy phase (a_0 = 0.3965 nm) and tetragonal SnO_2, while samples with the same composition but heat treated at 900 °C consisted of stoichiometric hexagonal PtSn, a nearly stoichiometric Pt_3Sn fcc phase (a_0 = 0.3988 nm), and tetragonal SnO_2. The 3:1 catalyst sample that was reduced in H_2 at 270 °C was composed entirely of the stoichiometric Pt_3Sn cubic phase (a_0 = 0.3998 nm) along with some unreacted SnO_2. The fact that hexagonal PtSn is not observed in Pt−Sn catalyst unless the material is heat treated at high temperature was also evidenced by Colmati et al., who showed that this phase is unequivocally observed in Pt:Sn (75:25) electrocatalyst prepared by the formic acid method only after the material was heat treated for 1 h at 500 °C in a flowing H_2 atmosphere.[18]

PtSn is a hexagonal phase (*P*63/*mmc,* 194) with lattice parameters a = 0.4104 nm and c = 0.5436 nm. The main diffraction peak of that phase occurs at $2\theta = 42°$ and 46 ° (there are other peaks, but they are less intense). As far as we can tell from the XRD patterns of Figure 2, there are no discernible peaks at those positions that could be attributed to a hexagonal PtSn phase. This is consistent with the fact that this phase is only observed after treatment at high temperature.[18,36] However, it must be recognized that the contribution of the C support to the diffraction pattern is quite significant at these angles and that the presence of a small amount of a hexagonal PtSn phase cannot be totally ruled out.

Following the analysis of Colmati et al.,[18] the Sn content of the fcc phase was determined using Vegard's law. For this purpose, the value of the lattice parameter (a_s) of pure Pt_3Sn was used (a_s = 0.40 nm), while the lattice parameter of $Pt_{100}Sn_0$ catalyst (a_0 = 0.391 nm), taken from Figure 3, was used. With these values x can be calculated with the following relationship

$$x = [(a-a_0)/(a_s-a_0)]x_s$$

where x_s is the Sn atomic fraction (0.25) of the Pt_3Sn catalyst, a is the lattice parameter of the fcc phase (taken from Figure 3), and x is the Sn atomic fraction of that phase. In the case of Pt_xSn_{100-x} elaborated in vacuum, the Sn content of the fcc phase reaches a maximum of 0.03 (compared to 0.25 for Pt_3Sn). In comparison, the Sn content of the fcc phase of Pt_xSn_{100-x} elaborated in 2 Torr He increases steadily from 0 to 0.13 as $[Pt]_{bulk}$ varies from 100 to 50 atom %. There is a marked difference between the bulk Sn content (as determined by EDX analysis) and the Sn content of the fcc phase. As noticed before, metallic tin is observed in the XRD patterns of Pt_xSn_{100-x} elaborated in vacuum and 2 Torr He. Closer inspection of Figure 2 reveals that the intensities of Sn(200) and Sn(101) (occurring at $2\theta = 30.6°$ and 32.0°, respectively) are more important in the XRD patterns of Pt_xSn_{100-x} catalysts elaborated in vacuum than they are in the patterns of the same material prepared in 2 Torr He. This is consistent with the fact that less Sn is found in the fcc phase of the former catalysts than in the later ones.

The average crystallite size was estimated from the width of the Pt(111) diffraction peak using the Debye−Scherrer equation. These results are presented in Table 1. The crystallite sizes of samples prepared under vacuum varies from 12 to 14 nm. They are significantly larger than those of samples prepared at 2 Torr He, which are closer to 8−9 nm. In PLD, the deposition conditions, notably the pressure in the deposition chamber and nature of the background gas, have a profound influence on the energies of the species being deposited on the substrate. This is especially so of the crystallite size, and in the case of Au, it was shown that the crystallite size increases steadily with the kinetic energy of the species being deposited.[37] This is thought

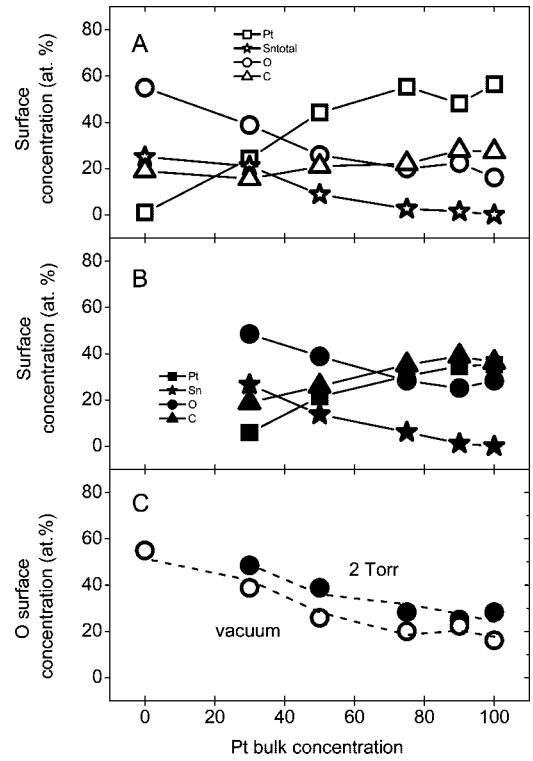

Figure 4. Variation of the surface concentration of Pt_xSn_{100-x} catalysts deposited under vacuum (A) and 2 Torr He (B) with respect to the Pt bulk concentration. (C) Variation of the experimental (symbols) and calculated (line) O surface concentration.

to arise as a consequence of the increased surface mobility of species deposited at higher kinetic energy. It is hypothesized that the same applies in the case of the Pt−Sn catalysts prepared in the present study and that the increased crystallite size of Pt−Sn samples prepared under vacuum originates from the higher kinetic energy of the species being deposited.

3.4. XPS Analysis. The atomic surface concentrations of Pt_xSn_{100-x} catalysts were determined by X-ray photoelectron spectroscopy. To achieve this, the whole surface area under the Pt 4f, C 1s, O 1s, and Sn 3d core level peaks was used. Figure 4A and 4B shows the variation of the Pt, C, O, and Sn surface concentrations with respect to the Pt bulk concentration of Pt_xSn_{100-x} catalysts prepared under vacuum and 2 Torr He, respectively. In both cases, the $[Pt]_{surf}$ increases with $[Pt]_{bulk}$, while $[C]_{surf}$, $[Sn]_{surf}$, and $[O]_{surf}$ decreases. From these measurements the surface concentration ratio $[Pt]_{surf}/[Pt]_{surf} + [Sn]_{surf}$ was extracted and plotted against the Pt bulk concentration (see Figure 3B). As seen in that figure, catalysts prepared under 2 Torr He have a surface composition that closely follows the bulk concentration. Thus, these samples possess a homogeneous composition and no surface segregation occurs. In contrast, the Pt surface composition of samples prepared in vacuum exceeds the Pt bulk composition. For deposition performed in vacuum, Pt is clearly segregated at the surface of the samples. This segregation effect is maximal for $[Pt]_{bulk}$ close to 50%.

As shown elsewhere, the kinetic energy of the plasma species formed during the pulsed laser deposition process varies with the background pressure in the deposition chamber. In vacuum, the absence of collisions between the expanding plasma and the surrounding gas molecules yields to a situation where the kinetic energy of the plasma species is the highest. In contrast, the presence of an atmosphere in the deposition chamber will reduce the kinetic energy of the plasma species. This is due to that fact that the expanding plasma will interact more strongly with

the molecules of the gas. As the pressure in the deposition chamber is increased, the probability for the plasma species to lose part of their kinetic energy through an interaction (collision) with the gas molecules will also increased, thereby lowering the kinetic energy of the plasma species. Thus, increasing the pressure in the deposition chamber reduces the kinetic energy of the plasma species.

It has also been shown elsewhere that a variation of the kinetic energy of the plasma species yields to a change of the surface mobility of the deposited species.[38,39] Higher surface mobility of the deposited species translates into denser films and surface rearrangement that yield to minimization of the energy. This effect has been shown to operate during the deposition of noble metal films on mesoporous anodic oxide aluminum membrane.[39] In that case, film deposited at high kinetic energy reproduces the underlying mesoporous structure of the underlying substrate, while films deposited at lower kinetic energy do not. In the former case, the high kinetic energy and surface mobility of the deposited species allow them to minimize the surface energy, yielding to formation of mesoporous noble metal films that duplicate the underlying mesoporous structure of the substrate.

The surface energies of Pt and Sn are $\gamma_{Pt} = 2.34$ J cm^{-2} and $\gamma_{Sn} = 0.57$ J cm^{-2}, respectively. From a thermodynamic point of view, one would therefore expect Pt_xSn_{100-x} films deposited at high kinetic energy to show a Sn surface excess since this would minimize the energy of the system. This is not the case as Pt_xSn_{100-x} deposited in vacuum (high kinetic energy) has excess Pt at the surface.

Excess Pt at the surface of Pt_xSn_{100-x} deposited in vacuum could reflect the fact that the partial pressures of Sn and Pt are very different. The partial pressure of tin at 2336 K is 200 mmHg. For comparison, Pt reaches the same partial pressure at 4196 K. The equilibrium vapor pressure is an indication of a solid's evaporation rate. It relates to the tendency of molecules and atoms to escape from a solid. Therefore, since the partial vapor pressure of tin is much larger than Pt and given the high kinetic energy and surface mobility of the plasma species when deposition is performed in vacuum, it is hypothesized that excess Pt at the surface of Pt_xSn_{100-x} is a result of the higher evaporation rate of Sn compared to Pt. According to that hypothesis, Pt_xSn_{100-x} deposited under 2 Torr would not show a surface excess owing to the reduced atom mobility and, hence, evaporation rate compared to the same materials deposited in vacuum.

High-resolution Pt 4f core level spectra of pure Pt deposited under vacuum and 2 Torr He are shown as curves A and E of Figure 5, respectively. Both Pt 4f core level spectra display two peaks whose maximum intensities are located at ~71.3 and ~ 74.6 eV. These two maxima correspond to the Pt $4f_{7/2}$ and Pt $4f_{5/2}$ core level peaks, respectively. The binding energy difference ($\Delta E_{bind} = 3.3$ eV) between these two maxima is that expected from Pt $4f_{7/2}$ and Pt $4f_{5/2}$ core level peaks. The position of these two peaks is consistent with the fact that Pt is in a metallic state. They are shifted to higher binding energy compared to the Pt 4f XPS signal of bulk Pt metal.[40] This shift might be indicative of a significant contribution from metal−support interaction or small cluster size effects.[41]

Each core level peak was fitted using only one component with an asymmetric profile (see Figure 5). This is done to take into account the tailing at high binding energy of the core level peak of metals.[42,43] In the case of Pt, this phenomenon was observed on an Ar-etched Pt foil for which all carbon and oxygen contamination had been removed from the surface layer.[44] The same approach (use of an asymmetrically modified line shape) was followed by other authors.[45] However, there is no consensus in the literature, and other people have used a symmetric function to fit the metallic component of unsupported Pt−Ru catalysts.[46] In that case, use of a second or even a third additional doublet is needed to obtain a satisfactory fit of the experimental data.

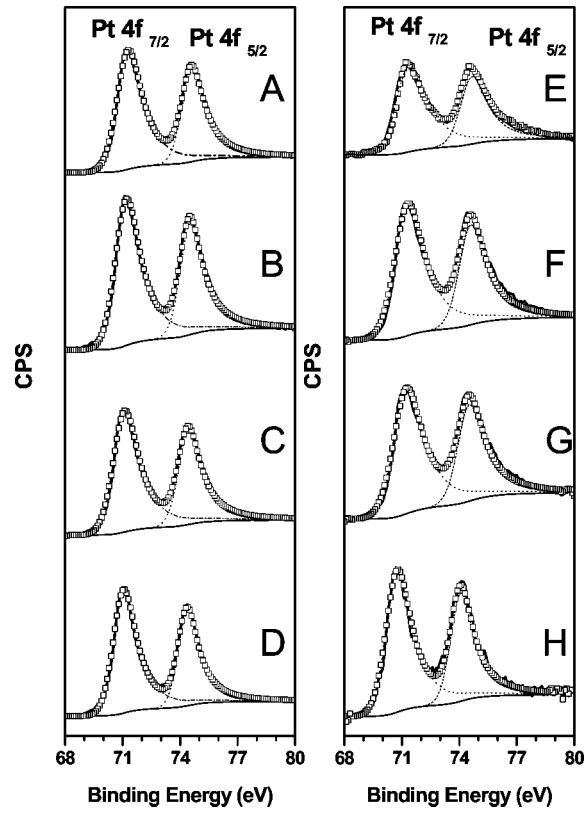

Figure 5. X-ray photoelectron spectra of the Pt 4f core level peaks of Pt_xSn_{100-x} catalysts deposited under vacuum (A−D) and 2 Torr He (E−H). The composition of the catalyst is (A and E) $Pt_{100}Sn_0$, (B and F) $Pt_{75}Sn_{25}$, (C and G) $Pt_{50}Sn_{50}$, and (D and H) $Pt_{30}Sn_{70}$.

TABLE 2: Parameters Extracted from Analysis of Pt Core Level XPS Spectra of Pt_xSn_{100-x} Catalysts

	under vacuum				under 2 Torr He			
catalyst	Pt 4f $_{7/2}$ (eV)	fwhm (eV)	Pt 4f $_{5/2}$ (eV)	fwhm (eV)	Pt 4f $_{7/2}$ (eV)	fwhm (eV)	Pt 4f $_{5/2}$ (eV)	fwhm (eV)
Pt	71.29	1.39	74.61	1.23	71.23	1.33	74.56	1.15
$Pt_{90}Sn_{10}$	71.25	1.38	74.77	1.23	71.37	1.45	74.69	1.28
$Pt_{75}Sn_{25}$	71.19	1.38	74.49	1.21	71.33	1.62	74.65	1.43
$Pt_{50}Sn_{50}$	71.09	1.40	74.42	1.23	71.26	1.63	74.55	1.42
$Pt_{30}Sn_{70}$	71.05	1.27	74.37	1.12	70.70	1.42	74.01	1.24

The Pt 4f $_{7/2}$ and Pt 4f $_{5/2}$ core level peaks of all Pt_xSn_{100-x} catalysts were fitted using the same procedure, and the fitting parameters are given in Table 2. The position of the Pt $4f_{7/2}$ core level peak of Pt_xSn_{100-x} catalysts deposited under vacuum varies by less than 0.24 eV from pure Pt to $Pt_{30}Sn_{70}$. In contrast, the position of the Pt $4f_{7/2}$ core level peak of Pt_xSn_{100-x} catalysts deposited under 2 Torr He varies by more than 0.5 eV as $[Pt]_{bulk}$ varies from 100 to 30 atom %. This is thought to reflect the fact that the maximum Sn content of the fcc phase of Pt_xSn_{100-x} catalysts prepared in vacuum is 0.03 compared to 0.13 for the same materials prepared in 2 Torr He. It is noteworthy that the shape of the Pt $4f_{7/2}$ and Pt $4f_{5/2}$ core level peaks does not evolve with the Pt content. In particular, there is no hint of a component at higher binding energy that would indicate the presence of Pt in a higher oxidation state.

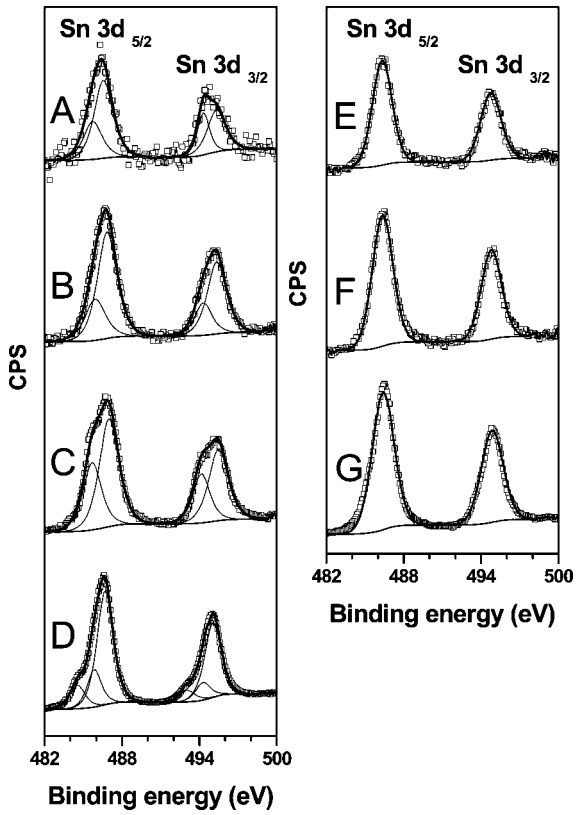

Figure 6. X-ray photoelectron spectra of the Sn 3d core level peaks of Pt_xSn_{100-x} catalysts deposited under vacuum (A-D) and 2 Torr He (E-G). The composition of the catalyst is (A and E) $Pt_{75}Sn_{25}$, (B and F) $Pt_{50}Sn_{50}$, (C and G) $Pt_{30}Sn_{70}$, and (D) Pt_0Sn_{100}.

The Sn 3d core level spectra of Pt_xSn_{100-x} catalysts deposited under vacuum and 2 Torr He are displayed in Figure 6. Both components (Sn $3d_{5/2}$ and Sn $3d_{3/2}$) of the Sn 3d core level spectra of Pt_xSn_{100-x} catalysts deposited under vacuum display a shoulder on the low binding energy side of the peak maxima that indicates that Sn is present in more than one oxidation state. Thus, two components have been used to fit the Sn $3d_{5/2}$ and Sn $3d_{3/2}$ core level spectra of catalysts deposited under vacuum, with the exception of Pt_0Sn_{100} (pure tin), which required a third component to account for the presence of a small amount of metallic tin. In contrast, there is no hint of a component on the low binding energy side of the peak maxima, and only one component is needed to fit the Sn 3d core level peaks of Pt_xSn_{100-x} catalysts prepared under 2 Torr He. The binding energies, full width at half-maximum (fwhm), and relative intensities of the various components are given in Tables 3 and 4.

The Sn 3d core level spectra of Pt_0Sn_{100} deposited under vacuum display three components. The one at lower binding energy occurs at ~484.5 eV and is associated with the presence of metallic tin.[40,47] The other two components occur at ~485.8 and ~486.7 eV. In vacuum, the Sn 3d core level spectra of the other Pt_xSn_{100-x} catalysts do not show evidence that metallic tin is present, and they display only the components occurring at higher binding energy. The one at ~485.5 eV accounts for ~35% of the total area under the 3d peaks, while the other one occurs at ~486.8 eV and accounts for ~65% of the total area. These two components have been found to occur at very similar binding energies in commercially available Pt−Sn catalyst.[48] It is difficult to discriminate between Sn(II) and Sn(IV) as the binding energies of these two oxides are close to each other.[49−51] Nevertheless, based on the work of Ansell et al.,[52] it is hypothesized that the higher binding energy component (~486.8 eV) is due to the presence of Sn^{4+} while the lower binding energy component (~485.5 eV) arises as a result of the presence of Sn^{2+} at the surface of the sample. As we shall see later on, this hypothesis is consistent with the [O]/[Sn] surface atomic ratio.

TABLE 3: Parameters Extracted from the Analysis of Sn Core Level XPS Spectra of Pt_xSn_{100-x} Catalysts Prepared under Vacuum

			$Pt_{75}Sn_{25}$	$Pt_{50}Sn_{50}$	$Pt_{30}Sn_{70}$	Sn
Sn $3d_{5/2}$	1st component	BE (eV)				484.5
		%[a]				13
		fwhm (eV)				1.41
	2nd component	BE (eV)	485.92	485.91	485.68	485.8
		%[a]	33	30	38	20
		fwhm (eV)	1.70	1.85	1.70	1.30
	3rd component	BE (eV)	486.74	486.83	486.98	486.7
		%[a]	67	70	62	67
		fwhm (eV)	1.68	1.75	1.76	1.46
Sn $3d_{3/2}$	1st component	BE (eV)				493.1
		%[a]				12
		fwhm (eV)				1.50
	2nd component	BE (eV)	494.44	494.31	494.16	494.3
		%[a]	37	30	38	15
		fwhm (eV)	1.60	1.57	1.55	1.35
	3rd component	BE (eV)	495.21	495.34	495.48	495.0
		%[a]	63	70	62	73
		fwhm (eV)	1.80	1.74	1.77	1.50

[a] Relative percentages of the first, second, and third component.

TABLE 4: Parameters Extracted from the Analysis of Sn Core Level XPS Spectra of Pt_xSn_{100-x} Catalysts Prepared under 2 Torr He

	Sn $3d_{5/2}$			Sn $3d_{3/2}$		
catalyst	BE (eV)	%	fwhm (eV)	BE (eV)	%	fwhm (eV)
$Pt_{75}Sn_{25}$	486.38	100	1.80	494.80	100	1.85
$Pt_{50}Sn_{50}$	486.39	100	1.90	494.82	100	1.85
$Pt_{30}Sn_{70}$	486.45	100	2.02	494.90	100	2.00

In contrast, the Sn 3d core level spectra of Pt_xSn_{100-x} catalysts deposited under 2 Torr He display only one component. It occurs at ~486.3 eV, which is less than the binding energy of the component attributed to Sn^{4+}. This suggests that the formal oxidation state of Sn is less than 4. Obviously, the formal oxidation state of tin differs according to the pressure in the deposition chamber.

The nature of the tin oxide that forms at the surface of Pt_xSn_{100-x} can be also appraised by considering the O surface concentration. As noted earlier, the O surface concentration decreases as the bulk Pt content increases, suggesting that Pt oxide is not a major constituent of the electrode surface. This suggests that there is a very little amount of oxidized platinum at the surface of the sample. This is consistent with the fact that no Pt oxide component was found under the Pt 4f core level peaks. Thus, the stoichiometry of the tin oxide, SnO_x, and oxidized carbon, CO_y (this notation is used as a short way to express the fact that C atoms at the surface of the sample bear an O containing groups), at the surface of the sample was estimated from the known surface concentration of (oxidized) tin and carbon atoms. To do this, the O surface concentration, $[O]_{cal}$, was calculated using the following function

$$[O]_{cal} = x[C] + y[\text{Sn oxide}]$$

where [C] is the C surface concentration, [Sn oxide] is the Sn surface concentration in an oxidized form, and x and y are the stoichiometry of the tin oxide (SnO_y) and oxidized carbon (CO_x). The values of x and y were obtained by a least mean square

procedure. In this way, it is implicitly assumed that the stoichiometry of SnO_y and CO_x are independent of the Pt bulk concentration. However, to account for a possible variation of x and y with the deposition conditions, the two sets of data (under vacuum and 2 Torr He) have been fitted independently. The results of the fit are shown in Figure 4C. As seen in that figure, the agreement between the calculated value and the experimental data is excellent. The values of x and y are 0.65 and 2.35 for Pt_xSn_{100-x} deposited under vacuum and 0.67 and 1.37 for Pt_xSn_{100-x} deposited at 2 Torr. It is interesting to note that an identical value of x (CO_x) has been found for the two sets of data. This is consistent with the fact that C at the surface of these samples must arise as a result of C contamination (adventitious contamination) and that the exact nature of this C contamination layer does not vary with the nature of the deposited layer. It is also noteworthy that the stoichiometry of tin oxide varies with the deposition conditions. In the case of Pt_xSn_{100-x} deposited under vacuum, the stoichiometry of the tin oxide is 2.37 compared to 1.37 for Pt_xSn_{100-x} deposited at 2 Torr He. This stoichiometry difference would reflect a change in the nature of the oxide formed at the surface of the catalysts with the background pressure in the deposition chamber. It is consistent with the difference observed previously between the Sn 3d core level peaks of Pt_xSn_{100-x} deposited under vacuum and 2 Torr He.

3.5. Cyclic Voltammetry. All catalysts have been tested electrochemically to evaluate their electrocatalytic activities for the electro-oxidation of ethanol. Cyclic voltammograms (CVs) of Pt_xSn_{100-x} catalysts prepared under vacuum and 2 Torr He are presented in Figure 7A and 7B, respectively. CVs were recorded from 0.05 to 0.70 V vs RHE to avoid the leaching of tin that occurs at more positive potential.[6,7,21] In this potential range, the stability of the surface of Pt_3Sn_1 (111) single crystal, in terms of both its structure and composition, has also been demonstrated.[53] Prior to measurements in ethanol, each electrode was electrochemically cleaned in sulfuric acid 0.5 M by cycling the electrode potential between 0.05 and 0.70 V vs RHE (scan rate = 50 mV s^{-1}). Superimposable CVs were obtained after 50 cycles, indicating that the surface has reached a steady state.[6] The 50th CV of each catalyst is shown in the insert of Figure 7A and 7B. Following that, the electrode was transferred to a H_2SO_4, 0.5 M + C_2H_5OH, 1 M electrolyte, and the cycling of the electrode potential was resumed (scan rate = 5 mV s^{-1}) and pursued as long as superimposable CVs were obtained. This was generally achieved after 5 cycles.

Two parameters were extracted from the CVs recorded in ethanol: the onset potential for ethanol oxidation, E_{onset}, and the current density at a fixed potential (0.5 V vs RHE), $j_{0.5}$. The variation of E_{onset} and $j_{0.5}$ with the Pt bulk concentration is depicted in Figure 8A and 8B, respectively. The onset potential is defined as the potential value at which the current reaches 10% of its value at 0.7 V vs RHE. The onset potential for ethanol oxidation on pure Pt is close to 0.500 V vs RHE, and almost identical values are obtained for pure Pt electrodes prepared in either vacuum or 2 Torr He. As shown elsewhere, the surface roughness and porosity of Pt prepared by PLD increase as the background pressure in the deposition chamber is increased.[38] These changes of the film porosity and surface roughness have a direct influence on the electrochemically active surface area that increases also with the pressure in the deposition chamber. However, the onset potential is an intensive parameter that should not vary with the electrochemically active surface area. Thus, the fact that identical E_{onset} values are found for Pt deposited under vacuum and 2 Torr He is not unexpected.

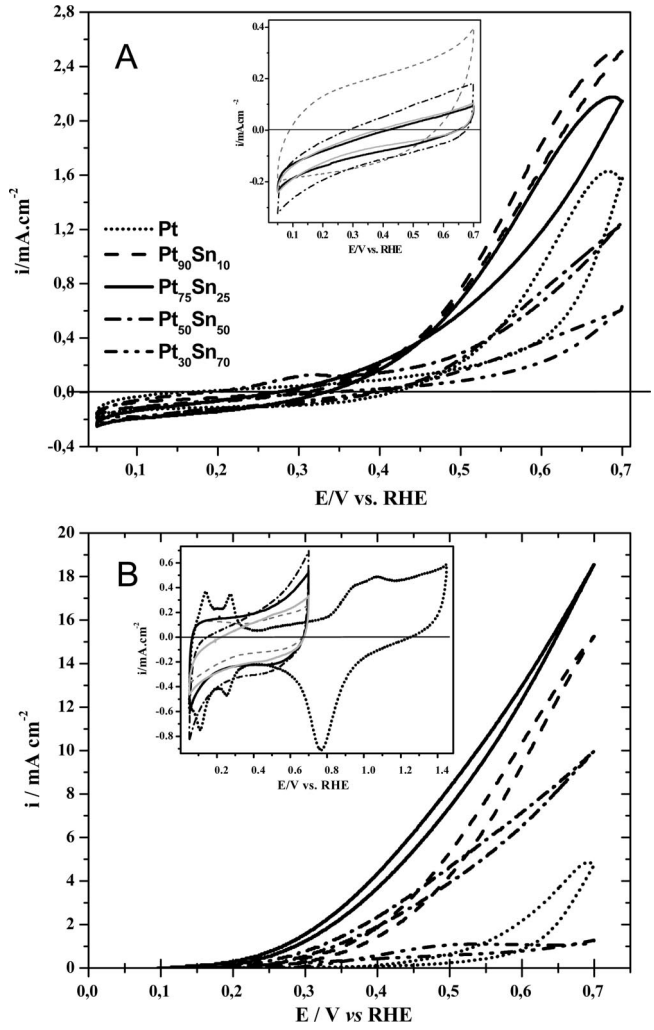

Figure 7. Cyclic voltammograms (CVs) of Pt_xSn_{100-x} catalysts elaborated under vacuum (A) and 2 Torr He (B). The CVS were recorded in H_2SO_4, 0.5 M + C_2H_5OH, 1 M (scan rate = 5 mV s^{-1}). (Insert) CVs of the same catalyst recorded in H_2SO_4, 0.5 M (scan rate = 50 mV s^{-1}). The current densities are given with respect to the geometrical areas.

Indeed, this indicates that the nature of the active sites at the surface of Pt deposited under these conditions is identical.

In contrast, the onset potential for ethanol oxidation varies with the Pt bulk content. For catalysts prepared in vacuum, E_{onset} is slightly lowered as $[Pt]_{bulk}$ is decreased from 100 to 50 atom %. It then increases again as $[Pt]_{bulk}$ reaches 30 atom %. A similar trend is observed for Pt_xSn_{100-x} prepared under 2 Torr He, except that the variation of E_{onset} is more marked than for the same catalyst compositions elaborated in vacuum. The E_{onset} value decreases from 0.56 to 0.31 V as $[Pt]_{bulk}$ varies from 100 to 75 atom %. At still lower $[Pt]_{bulk}$ value, E_{onset} stays constant. In both cases, the onset potential for ethanol oxidation is minimal in the vicinity of $Pt_{75}Sn_{25}$, indicating that the ratio of 3 Pt atoms for every Sn atom is the most efficient composition. A similar conclusion has been reached previously in other studies.[4,6,15,18,20]

The same conclusion can be reached by comparing the current density of the CVs at any given potential. For example, Figure 8B shows the variation of $j_{0.5}$ with respect to $[Pt]_{bulk}$. In both cases, $j_{0.5}$ values are maximal for $Pt_{75}Sn_{25}$. Also, the current density values of $Pt_{75}Sn_{25}$ prepared under 2 Torr He are about 10 times larger than that of the catalyst with the same composition prepared in vacuum. This is consistent with the fact that the E_{onset} value of the former catalyst is smaller (less

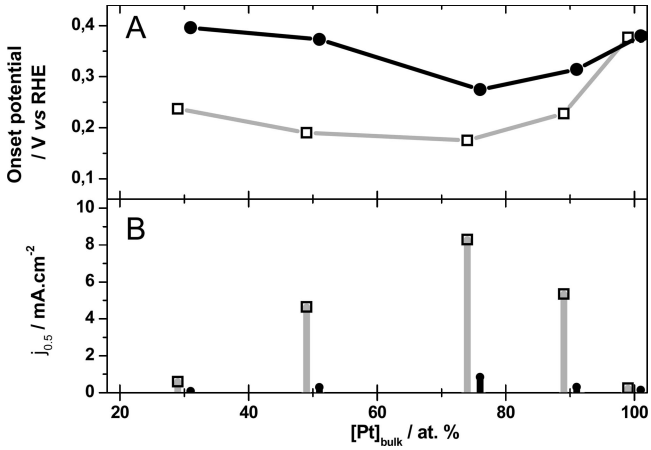

Figure 8. Variation of the (A) onset potentials, E_{onset}, and (B) current densities recorded at 0.5 V vs RHE, $j_{0.5}$, with respect the Pt bulk concentration of Pt_xSn_{100-x} prepared under vacuum (●) and 2 Torr He (□). The values of E_{onset} and $j_{0.5}$ were calculated from the CVs displayed in Figure 7. The current densities are given with respect to the geometrical areas.

anodic) than that of the latter. Thus, there is a beneficial effect of performing the deposition of PtSn catalyst in the presence of He.

As noted before, performing PLD under an He atmosphere has the effect of reducing the kinetic energy of the deposited species, yielding to films that are rougher and more porous. As shown elsewhere, this has a direct effect on the electrochemically active surface area. Thus, the larger $j_{0.5}$ values of catalysts prepared under 2 Torr He could well arise as a consequence of increased porosity and surface roughness compared to catalyst deposited at higher kinetic energy conditions (in vacuum). This would be consistent with the increased surface roughness observed in Figure 1 for films deposited under 2 Torr He.

To alleviate these concerns, the electrochemically accessible surface areas (EASA) of a few selected samples were measured. This was done by recording the CVs of the catalysts (in H_2SO_4) at several scan rates between and computing the capacitance of the electrode from the variation of the current with the sweep rate. A value of 20 μF cm^{-2} metal atoms was then used to calculate the EASA. This value has been determined on pure Pt electrode, and to the best of our knowledge, the specific capacitance of PtSn alloy surface is not known. Nevertheless, it will be used in the present study as we are mostly interested in normalization of the Pt-rich surface. The EASAs of four samples were measured, namely, pure Pt and $Pt_{75}Sn_{25}$ prepared in vacuum and 2 Torr He. The capacitance of these samples is given in Table 5. As seen in that table the capacitance of Pt prepared under vacuum (570 μF) is less than that of Pt prepared at 2 Torr He (980 μF). This is consistent with the fact that deposits of Pt prepared under vacuum are denser and have a lower surface roughness than those prepared at higher He background pressure. It is also interesting to note that the current densities of both Pt films do not differ by more than 5% of each other once proper normalization to account for the EASA is performed (see Table 5). This indicates that the nature of the catalytic sites at the surface of Pt does not vary with the background pressure in the deposition chamber. In comparison, there is a more than a 10-fold difference between the normalized current densities of $Pt_{75}Sn_{25}$ prepared in vacuum and 2 Torr He, reflecting the fact that the nature of the catalytic sites varies with the background pressure.

3.6. Chronoamperometric Curves. Chronoamperometric curves were recorded to check the long-term activity and stability of the catalysts. This was done by stepping the potential from the open circuit potential to 0.5 V vs RHE in 0.5 M H_2SO_4 + 1 M C_2H_5OH. The current density values were recorded for 1 h, and the resulting $i-t$ curves are shown in Figure 9A and 9B for Pt_xSn_{100-x} prepared under vacuum and 2 Torr He, respectively. These measurements were performed after recording the CVs in ethanol. All curves of Figure 9 have the same general shape with three different regions. In the first one, which lasts only a few minutes, the current drops rapidly. This region is followed by a second one where the current decrease is less steep. Finally, in the third region, the current reaches a steady-state value. The decrease of current in the first and second regions is attributed to a rapid increase of the surface coverage with partially oxidized species that results in poisoning of the Pt surface and diminution of its ability to oxidize ethanol.[5−7,10,21,22] In the case of pure Pt, this results in a very low steady-state current density.

The effect of Sn on the steady-state current density is best appreciated in Figure 10 by plotting the value of $j_{0.5}$ after 1 h of electrolysis. As seen in Figure 10, mixing tin with Pt increases the steady-state current density. In both cases, the steady-state current density displays a maximum for $Pt_{75}Sn_{25}$. However, there is a factor of 10 difference between both sets of values, and a much higher activity is observed for catalysts prepared under 2 Torr He. This factor is not modified when the EASAs are taken into account (see Table 5).

4. Discussion

The structure of Pt_xSn_{100-x} catalysts investigated here differs according to the background pressure in the deposition chamber. For deposition performed under vacuum, a very small fraction (less than 3 atom %) of Sn atoms are dissolved in the bulk of the fcc phase. This amount is probably even less at the surface of the catalysts since it is enriched with platinum atoms. From XPS, the [O]/[Sn] atomic ratio is close to 2, suggesting that most Sn atoms are present as SnO_2. Accordingly, the surface of Pt_xSn_{100-x} prepared under vacuum most probably consists of a mixture of Pt fcc (with less than 3 atom % of Sn dissolved in it) and SnO_2. Increased activity of mixtures of Pt and SnO_2 for ethanol electro-oxidation has been reported elsewhere even if an alloyed phase between Pt and Sn is not formed.[5,23,54] In addition, there are reports of a promotional effect for H_2/CO electro-oxidation of carbon-supported Pt impregnated with nonalloyed SnO_x phase(s).[55,56] This is thought to arise since Sn nucleates oxygenated species which then react with adsorbed CO on Pt atoms. The physical contact between the SnO_x and Pt phases is an essential requirement for a synergistic or

TABLE 5: Normalized Value of the Electrochemical Activity for Ethanol Oxidation

catalysts	capacitance (μF)	$j_{0.5}$ (mA cm^{-2} geo)	normalized $j_{0.5}$ (μA cm^{-2} real)	steady-state $j_{0.5}$ (mA cm^{-2} geo)	normalized steady-state $j_{0.5}$ (μA cm^{-2} real)
Pt under vacuum	570	0.15	1.05		
Pt 2 Torr He	980	0.24	0.98		
$Pt_{75}Sn_{25}$ under vacuum	660	0.85	5.15	0.49	2.96
$Pt_{75}Sn_{25}$ 2 Torr	510	8.30	65.10	4.24	33.25

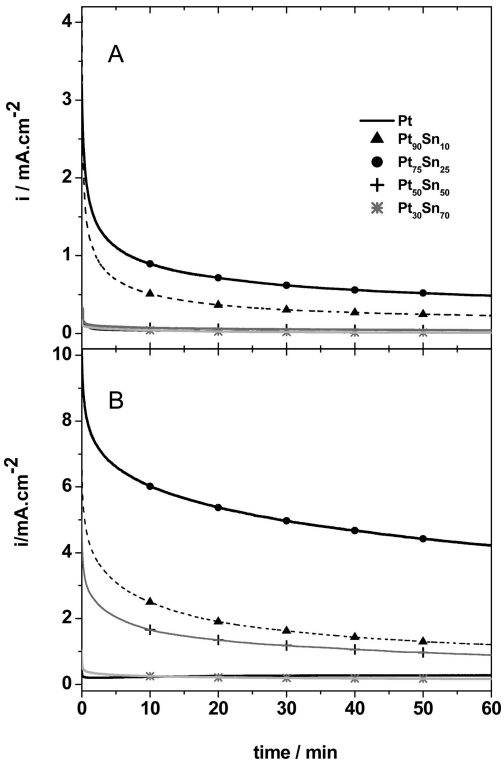

Figure 9. Evolution of the current density with time (recorded at 0.5 V vs RHE) for Pt_xSn_{100-x} catalysts prepared under vacuum (A) and 2 Torr He (B). The measurements were done in H_2SO_4, 0.5 M + C_2H_5OH, 1 M. The current densities are given with respect to the geometrical areas.

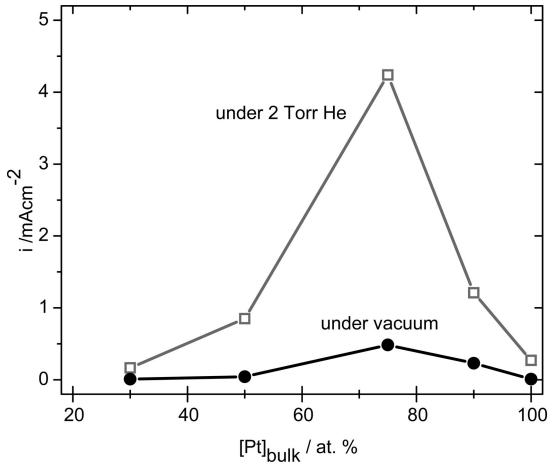

Figure 10. Variation of the steady-state current density with respect to the Pt bulk concentration of Pt_xSn_{100-x} catalysts prepared under vacuum (●) and 2 Torr He (□). The current densities were measured after 1 h of electrolysis at 0.5 V vs RHE in H_2SO_4, 0.5 M + C_2H_5OH, 1 M. The current densities are given with respect to the geometrical areas.

"promotional" effect. In the case of PLD, this would come as a given. The increased catalytic activity of Pt_xSn_{100-x} catalysts prepared under vacuum as x is increased from 0 to 25 can thus be rationalized even if a significant fraction of the tin atoms are not intimately mixed with Pt atoms.

For deposition performed under 2 Torr He, XRD analysis has shown that up to 13 atom % of Sn atoms are dissolved in the bulk of the fcc phase. As shown elsewhere, the surface composition and structure of single-crystal Pt_3Sn is that expected for the bulk termination surface structure.[53] Assuming the same holds true in the case of Pt-rich Pt−Sn alloys, this would mean that Pt and Sn atoms are mixed at the atomic level at the surface of the catalysts. In the case of Pt_xSn_{100-x} prepared under 2 Torr He, there is no segregation of Pt atoms at the surface of the catalysts. Moreover, it was shown by XPS that the [O]/[Sn] atomic ratio is 1.37, much lower than for catalysts with the same composition prepared under vacuum. This suggests that SnO_2 is not a major component of the catalysts prepared under 2 Torr He. As shown elsewhere by a temperature-programmed reduction profile, Sn^{2+} and Sn^{4+} can be found in Pt/Sn catalysts according to the preparation procedure.[57] Thus, a modification of the formal oxidation state of tin with the preparation conditions is not unexpected. In the case of catalysts prepared under 2 Torr He, it is hypothesized that this change in the formal oxidation state of tin is the result of Sn atoms being mixed at the atomic level with Pt atoms. As shown elsewhere, chemisorption of oxygen adatom on Pt_3Sn (111) single crystal is occurring on every other Sn atom.[53] Assuming that the oxidation results in ultrahigh vacuum apply to an electrochemical environment (the Sn atoms exists in two different chemical forms in the Pt_3Sn (111) surface) Stamenkovic et al.[53] were able to explain the occurrence of a high- and low-frequency CO_{ad} band in the FTIR spectra of the surface in contact with a CO-saturated 0.5 M H_2SO_4. They attributed the high-frequency band to CO adsorbed on Pt atoms adjacent to OH_{ad} covered Sn atoms and the low-frequency band to CO adsorbed on Pt sites in the vicinity of nonoxidized Sn atoms. The occurrence of Sn atoms in two different states at the surface of Pt_xSn_{100-x} catalysts is consistent with the fact the [O]/[Sn] atomic ratio is closer to 1 in catalysts prepared under 2 Torr He.

Gasteiger et al. have shown that Pt_3Sn single crystals have one of the highest catalytic activities for CO oxidation in acid solutions.[58,59] It was proposed that the significant enhancement provided by alloying Pt with Sn atoms can be ascribed to a combination of both bifunctional and ligand (electronic effects). It is proposed that the increased electrocatalytic activity of Pt_xSn_{100-x} catalysts prepared under 2 Torr He is due to the fact that a true Pt−Sn surface alloy is formed during the deposition. While a higher catalytic activity for CO oxidation resulting from the alloying of Sn with Pt is certainly a factor, it must not be forgotten that incorporation of Sn increases the lattice constant of the fcc phase. Zhou et al. suggested that a change (increase) of the Pt lattice parameter might favor adsorption of ethanol and C−C bond cleavage.[8] A detailed EQCM investigation of the mechanisms underlying the electrooxidation of ethanol on Pt_xSn_{100-x} catalysts prepared in different conditions is underway.

5. Conclusions

A series of Pt_xSn_{100-x} catalysts with different [Pt]/[Sn] ratios was prepared by the pulsed laser deposition method by varying the background pressure during the deposition. It was shown that this parameter has a profound influence on the surface composition and structure of the resulting catalysts. In turn, this has a marked effect on the electrocatalytic activity of the catalysts for ethanol oxidation. The best catalysts had a [Pt]/[Sn] ratio close to 3 and were prepared under 2 Torr He. It is hypothesized that increasing the background pressure from vacuum to 2 Torr He reduced the kinetic energy and surface mobility of the deposited species, thereby favoring formation of a true alloy at the surface of the catalyst.

Acknowledgment. This work was supported by the Natural Sciences and Engineering Research Council of Canada (NSERC) through a Strategic Grant, the Canadian Foundation for Innovation (CFI), the Fonds Québécois de la Recherche sur la Nature et les technologies (FQRNT), and INRS-ÉMT.

References and Notes

(1) Lamy, C.; Léger, J.-M.; Srinivasan, S. Direct Methanol Fuel Cells-from a 20th century electrochemists' dream to a 21st century emerging technology. In *Modern Aspects of Electrochemistry*; Bockris, J. O'M., Conway, B. E., Eds.; Plenum Press: New York, 2000; Vol. 34.

(2) Lamy, C. ; Léger, J.-M. In *Proceedings of the 2nd international Symposium on New Materials for fuel Cell and Modern Battery Systems*; Savadogo, O., Roberge, P. R., Eds.; Ecole Polytechnique: Montréal, 1997; p 477.

(3) Song, S.; Tsiakaras, P. *Appl. Catal.* **2006**, *63*, 187.

(4) Vigier, F.; Coutanceau, C.; Hahn, F.; Belgsir, E. M.; Lamy, C. *J. Electroanal. Chem.* **2004**, *563*, 81.

(5) Jiang, L.; Sun, G.; Sun, S.; Liu, J.; Tang, S.; Li, H.; Zhou, B.; Xin, Q. *Electrochim. Acta* **2005**, *50*, 5384.

(6) Siné, G.; Foti, G.; Comninellis, Ch. *J. Electroanal. Chem.* **2006**, *595*, 115.

(7) Colmenares, L.; Wang, H.; Jusys, Z.; Jiang, L.; Yan, S.; Sun, G. Q.; Behm, R. J. *Electrochim. Acta* **2006**, *52*, 221.

(8) Zhou, W. J.; Zhou, B.; Li, W. Z.; Zhou, Z. H.; Song, S. Q.; Sun, G. Q.; Xin, Q.; Douvartzides, S.; Goula, M.; Tsiakaras, P. *J. Power Sources* **2004**, *126*, 16.

(9) Zhou, W. J.; Song, S. Q.; Li, W. Z.; Zhou, Z. H.; Sun, G. Q.; Xin, Q.; Douvartzides, S.; Tsiakaras, P. *J. Power Sources* **2005**, *140*, 50.

(10) Spinacé, E. V.; Linardi, M.; Oliveira Neto, A. *Electrochem. Commun.* **2005**, *7*, 365.

(11) Zhou, W. J.; Song, S. Q.; Li, W. Z.; Sun, G. Q.; Xin, Q.; Kontou, S.; Poulianitis, K.; Tsiakaras, P. *Solid State Ionics* **2004**, *175*, 797.

(12) Jiang, L.; Sun, G.; Zhou, Z.; Zhou, W.; Xin, Q. *Catal. Today* **2004**, *93*, 665.

(13) Song, S. Q.; Zhou, W. J.; Zhou, Z. H.; Jiang, L. H.; Sun, G. Q.; Xin, Q.; Leontidis, V.; Kontou, S.; Tsiakaras, P. *Int. J. Hydrogen Energy* **2005**, *30*, 995.

(14) Léger, J.-M.; Rousseau, S.; Coutanceau, C.; Hahn, F.; Lamy, C. *Electrochim. Acta* **2005**, *50*, 5118.

(15) Lamy, C.; Rousseau, S.; Belgsir, E. M.; Coutanceau, C.; Léger, J.-M. *Electrochim. Acta* **2004**, *49*, 3901.

(16) Rousseau, S.; Coutanceau, C.; Lamy, C.; Léger, J.-M. *J. Power Sources* **2006**, *158*, 18.

(17) Colmati, F.; Antolini, E.; Gonzalez, E. R. *J. Electrochem. Soc.* **2007**, *154*, B39.

(18) Colmati, F.; Antolini, E.; Gonzalez, E. R. *Appl. Catal. B, Environ.* **2007**, *73*, 106.

(19) Bommersbach, P.; Mohamedi, M.; Guay, D. *J. Electrochem. Soc.* **2007**, *154*, B876.

(20) Colmati, F.; Antolini, E.; Gonzalez, E. R. *J. Power Sources* **2006**, *157*, 98.

(21) Wang, H.; Jusys, Z.; Behm, R. J. *J. Power Sources* **2006**, *154*, 351.

(22) Tanaka, S.; Umeda, M.; Ojima, H.; Usui, Y.; Kimura, O.; Uchida, I. *J. Power Sources* **2005**, *152*, 34.

(23) Mann, J.; Yao, N.; Bocarsly, A. B. *Langmuir* **2006**, *22*, 10432.

(24) Umeda, M.; Ojima, H.; Mohamedi, M.; Uchida, I. *J. Power Sources* **2004**, *136*, 10.

(25) *Pulsed Laser Deposition of Thin Films*; Chrisey, D. B., Hubler, G. K.,Eds.; Wiley: New York, 1994.

(26) Irissou, E.; Le Drogoff, B.; Chaker, M.; Guay, D. *J. Appl. Phys.* **2003**, *94*, 4796.

(27) Bommersbach, P.; Mohamedi, M.; Guay, D. Symposium on Electrochemistry of Novel Electrode Materials for Energy Conversion and Storage. *ECS Transactions*; Weidner, J., Dudney, N., Minteer, S., Zaghib, K., Eds.; The Electrochemical Society: Pennington, NJ, 2008; Vol. 6, Issue 25, pp 217−223.

(28) Irissou, E.; Vidal, F.; Johnston, T.; Chaker, M.; Guay, D.; Ryabinin, A. N. *J. Appl. Phys.* **2006**, *99*, 034904.

(29) Shirley, D. A. *Phys. Rev. B* **1972**, *5*, 4709.

(30) Kuznetsov, V. I.; Belyi, A. S.; Yurchenko, E. N.; Smolikov, M. D.; Protasova, M. T.; Zatolokina, E. V.; Duplayakin, V. K. *J. Catal.* **1986**, *99*, 159.

(31) Srinivasan, R.; De Angeles, N. J.; Davis, B. H. *J. Catal.* **1987**, *106*, 449.

(32) Srinivasan, R.; De Angeles, N. J.; Davis, B. H. *J. Catal. Lett.* **1990**, *4*, 303.

(33) Srinivasan, R.; Rice, L. A.; Davis, B. H. *J. Catal.* **1991**, *129*, 257.

(34) Srinivasan, R.; Davis, B. H. *Appl. Catal.* **1992**, *87*, 45.

(35) Srinivasan, R.; Sharma, R.; Su, S.; Davis, B. H. *Catal. Today* **1994**, *21*, 83.

(36) Radmilovic, V.; Richardson, T. J.; Chena, S. J.; Ross, P. N., Jr. *J. Catal.* **2005**, *232*, 199.

(37) Irissou, E.; Le Drogoff, B.; Chaker, M.; Trudeau, M.; Guay, D. *J. Mater. Res.* **2004**, *19*, 950.

(38) Irissou, E.; Hamel, C.; Laplante, F.; Dolbec, R.; Riabinina, D.; Le Drogoff, B.; El Khakani, M. A.; Rosei, F.; Chaker, M.; Guay, D. *J. Phys. Chem. C* Manuscriptin preparation.

(39) Pereira, A.; Laplante, F.; Chaker, M.; Guay, D. *Adv. Funct. Mater.* **2007**, *17*, 443.

(40) Wagner, C. D.; Riggs, W. M.; Davis, L. E.; Moulder, J. F. In *Handbook of X-ray Photoelectronic Spectroscopy*; Muilenberg, G. E., Ed.; Perkin Elmer Corp.: Eden Prarie, Minnesota, 1993.

(41) Eberhardt, W. E.; Fayet, P.; Cox, D. M.; Fu, Z.; Kalder, A.; Sherwood, R.; Sondericker, D. *Phys. Rev. Lett.* **1990**, *64*, 780.

(42) Niemantsverdriet, J. W. *Spectroscopy in Catalyst, An Introduction*; VCH Publishers: New-York, 1993.

(43) Doniach, S.; Sunjic, M. *J. Phys. C* **1970**, *3*, 285.

(44) Lalande, G.; Denis, M. C.; Guay, D.; Dodelet, J. P.; Schulz, R. *J. Alloys Compd.* **1999**, *292*, 301.

(45) Liu, R.; Iddir, H.; Fan, Q.; Hou, G.; Bo, A.; Ley, K. L.; Smotkin, E. S.; Sung, Y. E.; Kim, H.; Thomas, S.; Wieckowski, A. *J. Phys. Chem. B* **2000**, *104*, 3518.

(46) Aricò, A. S.; Antonucci, P. L.; Modica, E.; Baglio, V.; Kim, H.; Antonucci, V. *Electrochim. Acta* **2002**, *47*, 3723.

(47) Ansell, R. O.; Dickinson, T.; Povey, A. F.; Sherwood, P. M. A. *J. Electron Spectrosc. Relat. Phenom.* **1977**, *11*, 301.

(48) Shukla, A. K.; Arico, A. S.; El-Khatib, K. M.; Kim, H.; Antonucci, P. L.; Antonucci, V. *Appl. Surf. Sci.* **1999**, *137*, 20.

(49) Neri, G.; Rizzo, G.; Arico, A. S.; Crisafulli, C.; De Luca, L.; Donato, A.; Musolino, M. G.; Pietropaolo, R. *Appl. Catal., A* **2007**, *325*, 15.

(50) Ruiz-Martinez, J.; Sepulveda-Escribano, A.; Anderson, J. A.; Rodriguez-Reinoso, F. *Catal. Today* **2007**, *123*, 235.

(51) Vilella, I. M. J.; de Miguel, S. R.; de Lecea, C. S. M.; Linares-Solano, A.; Scelza, O. A. *Appl. Catal., A* **2005**, *281*, 247.

(52) Ansell, R. O.; Dickinson, T.; Povey, A. F.; Sherwood, P. M. A. *J. Electrochem. Soc.* **1977**, *124*, 1360.

(53) Stamenkovic, V. R.; Arenz, M.; Lucas, C. A.; Gallagher, M. E.; Ross, P. N.; Markovic, N. M. *J. Am. Chem. Soc.* **2003**, *125*, 2736.

(54) Simoes, F. C.; dos Anjos, D. M.; Vigier, F.; Léger, J. M.; Hahn, F.; Coutanceau, C.; Gonzalez, E. R.; Tremiliosi-Filho, G.; de Andrade, A. R.; Olivi, P.; Kokoh, K. B. *J. Power Sources* **2007**, *167*, 1.

(55) Goetz, M.; Wendt, H. *Electrochim. Acta* **1998**, *43*, 3637.

(56) Crabb, E. M.; Marshall, R.; Thompsett, D. *J. Electrochem. Soc.* **2000**, *147*, 4440.

(57) Liang, L.; Zhou, Z.; Li, W.; Zhou, W.; Song, S.; Li, H.; Sun, G.; Xin, Q. *Energy Fuels* **2004**, *18*, 866.

(58) Gasteiger, H. A.; Markovic, N. M.; Ross, P. N. *J. Phys. Chem.* **1995**, *99*, 8945.

(59) Gasteiger, H. A.; Markovic, N. M.; Ross, P. N., Jr. *Catal. Lett.* **1996**, *36*, 1.

JP801143A